Characterization of creep and creep damage by in-situ microtomography

András Borbély, Kristof Dzieciol, Federico Sket, Augusta Isaac, Marco Di Michiel, Thomas Buslaps, Anke R. Kaysser-Pyzalla

Characterization of Creep and Creep Damage by In-situ Microtomography

András Borbély, Krzysztof Dzieciol, Federico Sket, Augusta Isaac, Marco di Michiel, Thomas Buslaps, and Anke R. Kaysser-Pyzalla

Application of in-situ microtomography to characterization of power law creep and creep damage in structural materials is presented. It is shown first that the successively reconstructed volumes are adequately monitoring the macroscopic sample shape and that microtomography is an optimal tool to characterize inhomogeneous specimen deformation. Based on a two-step image correlation technique the evolution of single voids is revealed and the basis of a pioneering approach to creep damage studies is presented. The method allows the unequivocal separation of three concurrent damage mechanisms: nucleation, growth, and coalescence of voids. The results indicate that growth rate of voids with equivalent diameters in the range of 2–5 μm is of about one order of magnitude higher than the prediction of continuum solid mechanics. Analysis of void coalescence points out the presence of two stable growth regimes related to coalescence between primary and secondary voids, respectively.

INTRODUCTION

Synchrotron tomography is a relatively new investigation technique in materials science being frequently used after its spatial resolution reached the micrometer range.[1,2] It made possible the reconstruction of three-dimensional (3-D) representative volumes with sufficient microstructural details, necessary to predict the macroscopic properties of heterogeneous materials. For example the permeability of porous Fontainebleau sandstone estimated on the basis of a tomographic reconstruction showed good agreement with experimental data.[3] The method has been extensively used to visualize heterogeneous structures at the micrometer[4–8] and submicrometer scale with resolutions below 100 nm.[9,10] Work has been also oriented towards the use of high flux insertion devices with a broad energy spectrum, which led to the development of fast-tomography setups, capable of performing a full tomography scan in less than one second.[11] Fast-tomography systems are using white or pink radiation (filtered white radiation) produced by a wiggler or undulator source. Usually the lower part (E < 35 keV) of the energy spectrum is filtered out by placing an absorber in the direct beam. The photon flux falling on the detector remains, however, high and requires the use of reflecting optics. Due to the small x-ray absorption coefficient at high energies the absorbed dose is usually small; this is advantageous for studies of structural materials. The use of high energy radiation limits, however, the spatial resolution of fast-tomography reconstructions to about 2 μm[12] that is mainly related to the low efficiency of scintillator materials (YAG:Ce, LAG:Eu) at high energies when relatively thick scintillators have to be used.

In-situ fast-tomography during creep was carried out at beamline ID15A of the European Synchrotron Radiation Facility (ESRF). The highly intense "pink" synchrotron beam was generated by an asymmetric multipole wiggler (B_{max}=1.84T) delivering photon energies from 30 keV to 350 keV. The creep device with the sample was mounted on the goniometer of the tomograph and was rotated continuously by 180°. The transmitted intensity was recorded by a fast charge coupled device (CCD) camera working in frame transfer mode (DALSTAR 1M60) with a readout of 60 frames per second and allowed operation without mechanical shutter. Motorized slits defined the horizontal and vertical beam size of 1.7 mm and 1.3 mm, respectively. 800 radiographs with an exposure time of 250 ms each were collected in about 3 min.

The tomographic reconstructions were made with in-house developed

How would you…

…describe the overall significance of this paper?

An overview on the application of in situ tomography to creep and creep-damage studies is presented. Thanks to its nondestructive nature, the tomographic method allows a four dimensional characterization of deformation and damage processes in materials. We show that the growth rate of creep cavities in copper and brass is faster by one order of magnitude than predictions of the continuum theory.

…describe this work to a materials science and engineering professional with no experience in your technical specialty?

We show that in situ microtomography offers qualitatively new information about damage evolution in metals. Applying powerful image correlation algorithms to consecutively reconstructed volumes the growth and coalescence of single microvoids has been characterized. The results emphasize that void growth cannot be described by the continuum theory and suggest that local crystallography plays a crucial role.

…describe this work to a layperson?

Service lifetime of metallic components for high temperature applications is usually controlled by creep damage consisting of nucleation, growth and coalescence of grain boundary voids. Using the nondestructive method of microtomography we have followed the evolution of a huge number of voids in deformed copper and brass. It is shown that microtomography is an excellent tool for unequivocal characterization of growth and coalescence of single voids at the micrometer scale.

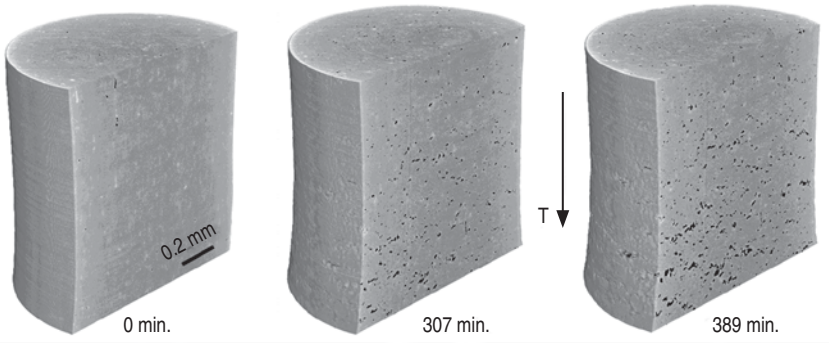

Figure 1. Tomographic reconstructions showing the distribution of damage at different creep times in Cu-40Zn-2Pb brass alloy. The specimen was exposed to a temperature gradient pointing towards the bottom of the sample. At higher temperatures damage accumulates faster due to higher local strain rates.

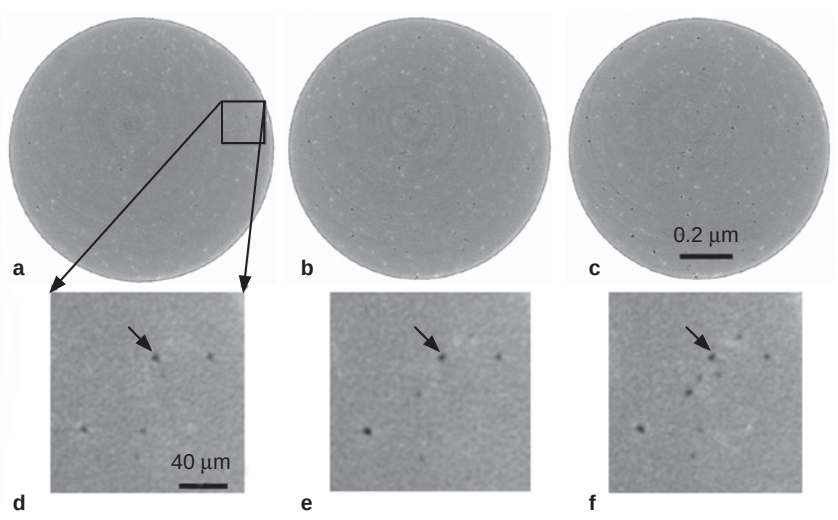

Figure 2. (a–c) Examples of slice registration and (d–f) area of interest (AOI) registration. The AOI registration corresponds to the void indicated by the arrow (see the paragraph on void growth).

software[13] accounting for characteristic noise reduction of the radiograms. Before reconstruction hot-spots were removed by comparing two subsequent projections, which are supposed to contain nearly the same information, so that they appear as outliers on the subtracted image. In a second step ring artifacts due to continuously excited detector sensors were suppressed using a "FFT filter" on the sinogram function. Since excited sensors produce horizontal streaks of a certain length along the angular axis, the sinogram was subdivided in 8 regions and each region was integrated along the angular axis so that the characteristic noise from constant sensor excitation could be well emphasized. The final reconstruction was also checked for eventual sample motion based on a comparison between forward (calculated from the reconstructed image) and original projections. Sample motion in the investigated case was negligible and did not need to be corrected.

This paper reports fast-tomography results describing creep and creep damage in oxygen free high conductivity copper and in the Cu-40Zn-2Pb (58wt.% Cu, 40wt.% Zn, and 2wt.%Pb) brass alloy, which contains three phases: α-brass, β-brass, and a lead rich particles. Three reconstructions showing the initial structure and damage in the tertiary creep stage of the brass alloy are shown in Figure 1.

CHARACTERIZATION OF THE KINETICS OF THE CREEP PROCESS

Creep deformation of metals at temperatures higher than about 1/3 of their melting temperature T_m is governed by several thermally activated processes enhancing dislocation motion and recovery, diffusion of vacancies as well as dynamic recrystallization.[14] These mechanisms influence mainly stage II of creep, where specimens under constant applied stress deform at nearly constant strain-rate. The relationship between this steady-state strain-rate and stress in pure metals and Class M alloys is often described by a power-law function:[14,15]

$$\dot{\varepsilon}_{ss} = C \cdot \left(\frac{\sigma(T)}{G(T)} \right)^n \cdot \exp\left(-\frac{Q_a}{R \cdot T} \right) \quad (1)$$

The pre-exponential factor C comprises structure-dependent parameters and is usually considered constant.[16] $\sigma(T) / G(T)$ is the local stress normalized by the shear modulus, n is the stress exponent, R is the gas constant and Q_a is the apparent activation energy of steady-state creep. The key parameters of this phenomenological description are n and Q_a, which once evaluated give a good indication about the main creep mechanism. Sherby et al.[17] have obtained the activation energy in pure aluminum over a large range of temperatures, from about $0.3 \cdot T_m$ to $0.9 \cdot T_m$. Their results confirm that above $0.6 \cdot T_m$, the activation energy Q_a, is comparable to that of lattice self-diffusion (Q_{sd}), but below $0.6 \cdot T_m$ is smaller than Q_{sd}.

The study of creep kinetics is based on Equation 1. It requires a cylindrical specimen with a temperature gradient applied along the external load. This means that material volumes at different temperatures, for example material slabs lying perpendicular to the direction of the temperature gradient and positioned at different heights in the gauge length, will deform at different rates. As temperature is in the argument of the exponential function the difference in strain rate among the slabs will be measurable even for temperature differences of a few degrees. The position of the slabs at different deformation states is obtained from successive tomographic reconstructions by 2-D image correlation (on the limiting upper and lower slices of the slab). An example of image correlation on a material slice in creep deformed brass is exemplified in Figure 2. It should be mentioned that the presence of voids helps image registration, leading to a higher cross correlation coefficient.[18]

Due to the good resolution of tomographic reconstructions (the sample diameter of 1 mm is measured typically with 2 μm accuracy) the change in the local cross sectional area and the related local strains and strain-rates can be accurately determined.[18–20] If the temperature difference between the slabs ΔT, is small compared to the applied temperature T then based on Equation 1 the logarithm of the strain-rate ratios of the slabs situated at the lowest temperature
T_0 and T can be approximated as:

$$\ln\left(\frac{\dot{\varepsilon}(T)}{\dot{\varepsilon}(T_0)}\right) \cong \frac{Q_a}{R \cdot T_0^2} \cdot \Delta T \qquad (2)$$

where the ratio of shear modulus normalized stresses was considered to be equal to one. Evaluation of the apparent activation energy requires, however, the knowledge of temperature distribution along the gauge length that can be obtained from finite element calculations combined with temperature calibration measurements. As shown in Figure 3 the logarithm of the normalized strain-rates (Equation 2) can be well fitted by a straight line, the slope of which yields the apparent activation energy. Evaluations based on the tomographic method provided results in good agreement with those obtained according to classical tests on standard specimens made of leaded brass[20] and AISI 440B steel.[19]

DAMAGE CHARACTERIZATION

High temperature creep damage has significant practical implications in high-end engineering applications, but especially in industries where high temperature loading occurs (e.g., in energy conversion processes) leading to unwanted and expensive shutdowns of power plants. It is known that service lifetime of metallic components is controlled by nucleation, growth and coalescence of grain boundary voids. Work on the subject culminated with a series of articles describing the evolution of the largest[21,22] or the i^{th} largest voids[23,24] found on the fracture surface of interrupted test specimens. The book of Riedel[25] gives a good overview about our current understanding in the field. Further theoretical developments are, however, difficult due to the absence of adequate experimental results corroborating the models. The reason for this is related to the complexity of damage, mainly due to its localized nature and superposition of the above-mentioned three different mechanisms. Nondestructive, statistical methods like small angle x-ray or neutron scattering are unlikely to deliver the right information due to the required extra assumptions on void shape and the relative contribution of the basic mechanisms to the total damage. In this work we describe how the nondestructive nature of in situ tomography can be used as a novel approach to void growth evaluation. Before that, however, we show the localized character of damage which emphasizes the inadequacy of damage theories based on average damage parameters.

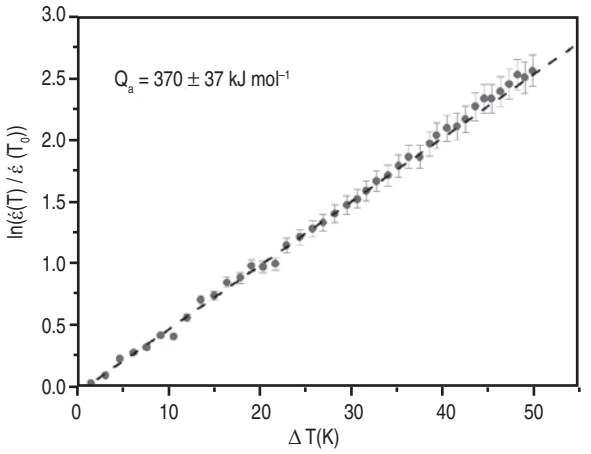

Figure 3. Variation of normalized strain rate as a function of temperature difference ΔT, along the gauge length of the specimen. T_0 represents the lowest temperature in the investigated volume and $\dot{\varepsilon}(T_0)$ the corresponding strain-rate. The slope of the fitted line is proportional to the apparent activation energy of stead-state creep (see Equation 2).

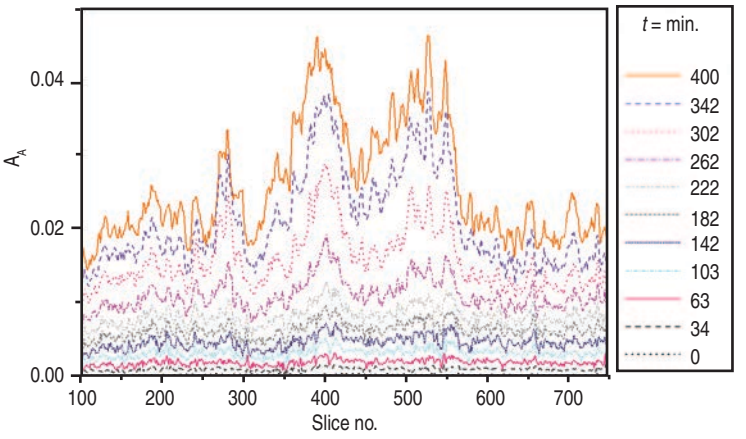

Figure 4. Distribution of the area fraction of voids on material slices lying perpendicular to the applied stress. Localization of damage on slices with initially higher volume fractions is noticeable. (OFHC copper creep deformed at 773 K).

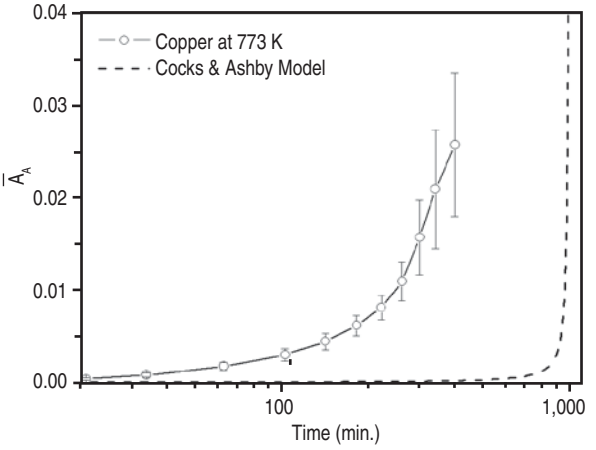

Figure 5. Evolution of the mean volume fraction of voids as a function of creep time. Comparison between experiment and the model of Cocks and Ashby.[26]

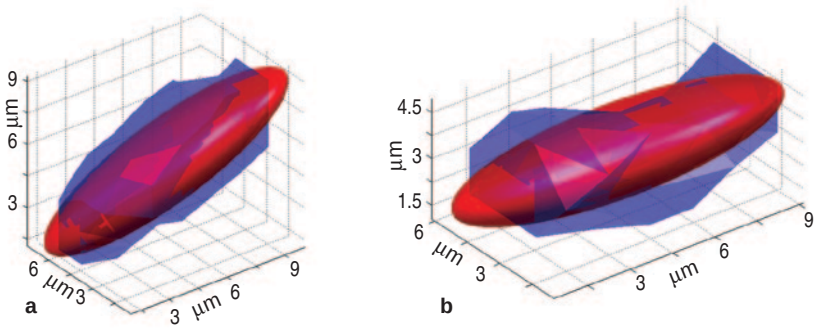

Figure 6. Illustration of two cavities and the corresponding equivalent ellipsoids. The related complexity factors are C= 0.5 and C = 1 for (a) and (b), respectively. For growth-rate evaluations only cavities with C < 0.6 were considered.

The simplest damage characterization concerns the growth of the area fraction (A_A) of voids, for which Cocks and Ashby have derived an analytical formula.[26,27] This quantity is obtained with high accuracy from tomographic slices facilitating a first comparison between experiment and models. Figure 4 shows the distribution of cavity area fraction on slices perpendicular to the external load as a function of slice position along the gauge length. The slice numbers refer to the initial state (t = 0) of a copper sample deformed at 773 K. At later times the area fraction represents the damage on the same material slice, which was displaced by creep, but identified by means of image correlation. The local evolution of A_A is remarkable, clearly emphasizing the localized and mainly deterministic character of damage. Small fluctuations become more and more accentuated with deformation, damage localizing to regions with initially higher amount of A_A. To compare these experimental findings with model prediction[26,27] the average area fraction $\overline{A}_A$ over all slices was calculated. The results are shown in Figure 5 as a function of creep time, where the model predictions were calculated by assuming that at zero time the initial area fraction is equal to the experimentally determined value of $2.3 \cdot 10^{-4}$. It is clear that the model underestimates the true amount of damage and overestimates time to rupture. It should be recalled, however, that the model does not take into account continuous cavity nucleation that takes place in reality, making difficult to draw a clear conclusion.

GROWTH RATE OF CREEP VOIDS

Due to aforementioned difficulties in interpretation of macroscopic damage parameters, the direct comparison between model and experiment requires the analysis of single cavities at the microscopic scale, where nucleation, growth and coalescence can be identified and separated. Owing to the large difference between x-ray attenuation coefficient of copper and air (as well as brass and air), tomographic images could be well segmented and voids were unequivocally identified in reconstructed volumes. Void identification was obtained with a two step image registration algorithm: (*i*) slice registration (Figure 2a–c) followed by (*ii*) area of interest (AOI) registration (Figure 2d–f). The AOI contained the selected void and its size was adjusted to include a few other voids, which helped cross-correlation.[18] The single void approach avoids per se the difficulties related to void nucleation, but to circumvent the influence of cavity coalescence extra conditions should be imposed. A common coalescence event between visible voids can be detected for example based on ancestor analysis. Coalescence between a visible void and those reaching the detection limit during the time interval between consecutive reconstructions requires, however, additional criteria. In the present case it has been assumed that such coalescence leads to a noticeable shape change. The complexity factor C describing cavity shape was introduced and defined on the basis of the exclusion volumes obtained from the intersection of the real cavity with its equivalent ellipsoid. C is equal to the ratio between the sum of the exclusion volumes (volumes belonging to the cavity or ellipsoid, but not to their intersection) and the cavity volume.[8] Based on a visual inspection of cavities shape the limit value of C = 0.6 was chosen to discern between non-coalesced and coalesced cavities. The selected C is not critical, C = 0.5 led practically to identical results, but the determined growth-rates had larger errors due to the smaller number cavities considered in the analysis. For C =

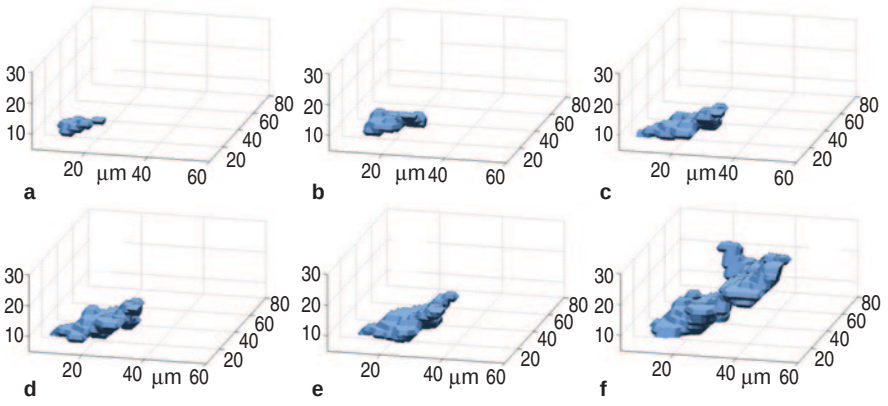

Figure 7. Shape evolution of a cavity growing along an inclined grain boundary in copper at different creep times. The creep times are (a) 60 min., (b) 113 min., (c) 233 min., (d) 299 min., (e) 352 min., and (f) 418 min.

1 the influence of coalescence on the growth rate of smaller voids was visible. Figure 6a and b shows two voids and their equivalent ellipsoids for which C = 0.5 and C = 1, respectively.

The evolution of a selected void growing along an inclined grain boundary is presented in Figure 7. The void is located at the center of the crept sample and lies initially nearly perpendicular to the stress axis (Figure 7a). The void grows, however, along an inclined grain boundary (Figure 7b–e). At the next triple junction branching of the void becomes visible (Figure 7f). The shape changes detected suggest that the void was initially located near a triple junction. Growth along the inclined grain boundary hints in addition that grain boundary sliding (GBS) might be the mechanism determining growth.

After identification of voids in consecutive tomographic reconstructions their growth-rate was calculated by dividing the change in void volume by the time interval between consecutive reconstructions, typically of 30 min. The selected approach allowed for the first time[28] checking the volume dependence of growth rates based on the continuum theory describing the growth of a hole in a nonlinearly viscous solid:[29]

$$\dot{V} = \Lambda \dot{\varepsilon} V \qquad (3)$$

where $\dot{V}$ is the volumetric growth-rate, V is the void volume and $\dot{\varepsilon}$ is the steady-state strain-rate. The proportionality factor Λ equals 3/4 and is of about unity for a spherical void in deforming linear and nonlinear solid, respectively.[25,29] The nonlinearly viscous material corresponds to the creeping polycrystal as characterized by the constitutive Equation 1. Such an equation was also proposed by Weertman based on the microscopic glide and climb process of dislocations.[30] Due to dislocation glide the local neighborhood of voids should play an important role in determining the growth rate and indeed a dependence on the crystallographic orientation of nearby grains was suggested on an empirical basis.[31] Since the continuum theory does not take into account these local inhomogeneities, the determined growth-rates were separated according to the volume of corresponding voids into size classes and the mean value for each class was calculated. During the analyzed creep interval of about 6 hours a growing void will have therefore contributions to the growth-rate of different size classes. To reduce the uncertainty of the results due to the limited resolution of microtomography (~1.5 voxels, or ~2 μm) evaluations were restricted only to voids with volumes larger than 15 voxels (1 voxel = 1.4^3 μm^3). The results both for copper and brass are shown in Figure 8, where the error bars represent the standard deviations of growth rates in each size class. They are much larger than the error of the segmentation method used to evaluate cavities volume, which is below 20%. We assume that these large standard deviations are related to the local void neighborhood, such as differences in local crystallography, void location at a simple grain boundary or at triple junction. This information is unfortunately not available from tomography. The number of analyzed growth rates was of about 75,000 and 12,000 for copper and brass, respectively.

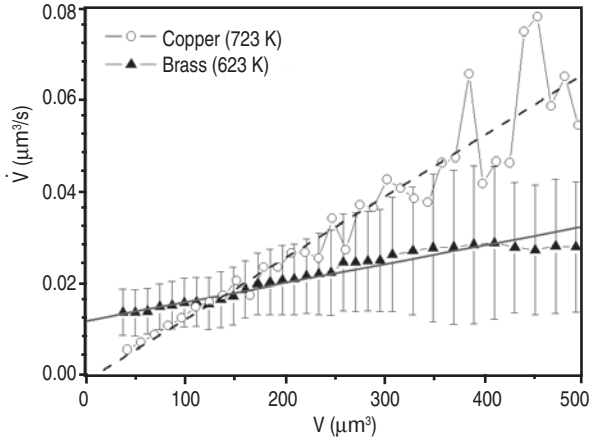

Figure 8. Growth rate of voids as a function of volume. Voids in OFHC copper obey Equation 3, while growth-rate of voids in brass has a positive intercept.

Comparing the theoretical growth rate (Equation 3) with Figure 8 the different growth behavior of voids in copper and brass can be noticed. While growth of voids in copper obeys the continuum law a deviation from the pure proportionality is found for brass. The non-zero intercept indicates that beside dislocation creep another mechanism, probably grain boundary diffusion, with significant contribution to the growth rate is also present. The grain boundary diffusion mechanism could not be unequivocally identified due to the complex structure of the leaded brass alloy for which no reliable material parameters characterizing grain boundary diffusion are available. Additionally, the lead rich zones located at grain boundaries are molten at the deformation temperature of 623K having the consequence that not only growing, but also shrinking voids were observed.[32] Shrinking of voids could be related only to the liquid lead phase, which expands during melting and progressively segregates along grain boundaries filling in nearby voids.

The most important experimental result is, however, related to the parameter Λ of the growth rate law (Equation 3), which was found much higher than the theoretically predicted $\Lambda \approx 1.1$.[29] Considering the slopes of the lines fitted in Figure 8 as well as the corresponding strain rates for steady-state creep, the experimental values of Λ are of about 45 and 28 for copper and brass, respectively. The result obtained is surprising at the first sight, but there are several indications that the continuum viscous solid model is not adequate to describe void growth during steady-state creep of polycrystals: (a) Riedel[25] has proposed a simple geometrical model to predict the strain to failure during power-law creep, but considering $\Lambda = 1.1$ he found (page 210 of Reference 25) an unrealistically high value of 383%. The much higher Λ obtained from experiment yields according to Riedel's model realistic fracture strains in good agreement with observations.[28] (b) From physical point of view it is not surprising that the form of Equation 3 is corroborated by experiments on pure copper. The equation can be also derived on a quite general basis

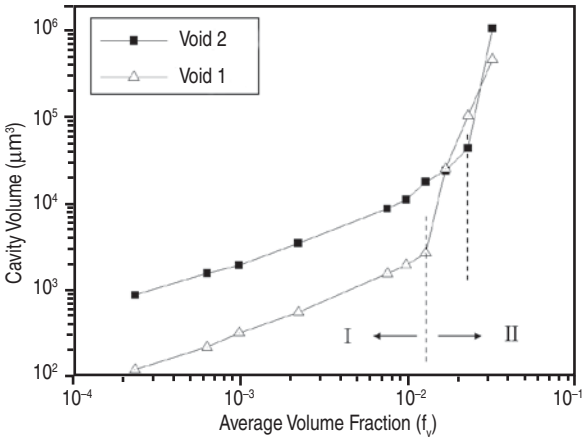

Figure 9. Volumetric growth of the two largest voids in brass. Coalescence with primary voids (regime I) and with secondary voids (regime II) is revealed. The transition between the two regimes takes place at volume fractions of about 1–3%.

by considering a dimensional analysis. The value of Λ, however, is related to the true growth mechanisms of the voids, which are dislocation glide and climb and are not explicitly considered in the viscous solid model. This means that even after averaging the growth-rates of voids in a size class, the obtained Λ may be different from the prediction of the continuum theory. Maire et al.[33] have shown that growth of large voids during room temperature deformation of a dual phase steel can be satisfactorily described by the Rice and Tracey model.[34] Considering copper and brass as plastically ideal materials as well as a uniaxial stress state the Rice and Tracey model predicts $\Lambda \approx 0.87$. Since at room temperature only dislocation glide takes place it suggests that contribution of dislocation glide to Λ is of the order of unity. Therefore we suppose that extra acting climb mechanism at high temperatures should lead to a higher Λ.

VOID COALESCENCE

Coalescence of voids is characteristic of later stages of creep and it is the basic mechanism of macro-crack formation leading to fracture. For ductile fracture at room temperature three different coalescence mechanisms have been proposed: (a) stable coalescence through impingement of primary voids, (b) unstable coalescence through shearing of the primary inter-void ligament and (c) coalescence of secondary voids across the primary inter-void ligaments also known as "void sheeting."[35] No experimental results are available for power law creep and it is open to discussion if the mechanisms of ductile fracture are valid. In situ tomography seems to be a very appropriate method for fracture investigations, too as documented by the large number of papers on the subject (see References 33, 36, and references therein). The technique allows for example a straightforward evaluation of void coalescence based on ancestor analysis. The ancestors of a given void in the current reconstruction are simply obtained by calculating the intersection between the volumes of the selected void with voids in the previous reconstruction. In this work we present the volumetric evolution of the two largest voids found in crept brass. The results are shown in Figure 9 as a function of the mean volume fraction of voids f_V (related to the investigated volume of about 0.8 mm^3) to facilitate their interpretation in terms of ductile damage models,[37,38] based on which fracture occurs when the mean volume fraction reaches a critical value. It is evident from Figure 9 that coalescence leads to faster growth than plastic creep (Equation 3, considering the experimental $\Lambda = 25$). The growth curve can divided in two regions as indicated by dotted vertical lines, which separate stable growth regimes characterizing coalescence between primary and secondary (formed by coalescence of primary voids) voids. In region I cavity volume depends almost linearly on f_V, while in region II a power law function with an exponent of about 4 to 5 is characteristic. The transition between the regions I–II takes place suddenly suggesting the existence of a critical volume fraction as proposed in ductile damage models.[37] For creep deformed brass at 623 K this critical value is at about 0.01–0.03, much smaller than usual values considered in ductile damage simulations of about 0.15. Tveergard and Needleman[38] proposed an extension of the Gurson's model by considering a second critical value of the void volume fraction, which has the role to describe accelerated damage after primary coalescence. In case of the largest voids studied here primary coalescence took place from the beginning of the test, and the detected critical volume fraction corresponds to the change in coalescence mechanism as proposed by Reference 38. It is generally agreed[35] that during fracture at room temperature voids typically coalesce through a combination of mechanisms (b) and (c) mentioned above. In contrast to this, present experimental findings show that during power law creep the beginning of void coalescence is characterized by a stable growth due to impingement of primary voids.

CONCLUSIONS

Tomographic reconstructions are similar to an accurate three-dimensional extensometer, which combined with the nondestructive nature of the technique, has led to new experimental results. In-situ monitoring the specimen macroscopic shape enabled the evaluation of the activation energy of creep on one single sample subjected to a temperature gradient. The used experimental setup is very flexible and other measurements with applied electric or magnetic fields can be also envisaged. Since the investigated material volume is small the tomographic method is attractive in cases when only a small amount of material is available.

In-situ microtomography allowed a fundamentally new approach to creep damage analysis. Following the evolution of single cavities the basic mechanisms of void nucleation, growth, and coalescence could be separated and the latter two individually studied. Experimentally found void growth rates are larger by at least one order of magnitude that the growth rate predicted by the continuum theory. The result indicates a physically plausible solution for the overly large strain to failure predicted the continuum theory. The large scatter of growth rates emphasizes in addition the importance of local crystallography, information unfortu-

nately not available from tomography. Analysis of void coalescence suggests the existence of two stable growth regimes described by impingement of nearby primary voids, followed by coalescence of secondary voids before final rupture.

ACKNOWLEDGEMENTS

The authors acknowledge the support of the Max-Planck Institute für Eisenforschung GmbH, Düsseldorf, Germany and the European Synchrotron Radiation Facility, Grenoble, France and of Prof. Dr. W. Reimers and Dipl. Ing. B. Camin of TU Berlin.

References

1. B.P. Flannery et al., *Science*, 237 (1987), pp. 1439–1444.
2. P. Spanne and L. Rivers, *Nucl. Instrum. Meth. Phys. Res.,* B-24/25 (1987), pp. 1063–1067.
3. P. Spanne et al., *Phys. Rev. Lett.,* 73 (1994), pp. 2001–2004.
4. L. Babout et al., *Acta Mater.,* 49 (2001), pp. 2055–2063.
5. A. Borbély et al., *Mater. Sci. Engng.,* A-367 (2004), pp. 40–50.
6. A. Pyzalla et al., *Science*, 308 (2005), pp. 92–95.
7. G. Requena et al., *Mater. Sci. Engng.,* A 487 (2008), pp. 99–107.
8. A. Isaac et al., *Mater. Sci. Engng.,* A-478 (2008), pp. 108–118.
9. R. Mokso et al., *Appl. Phys. Lett.,* 90 (2007), p. 144104.
10. G. Requena et al., *Scripta Mater.,* 61 (2009), pp. 760–763.
11. "High Energy Diffraction and Scattering Beamlines" (European Synchrotron Radiation Facility, 6 Rue Jules Horowitz, BP 220, 38043 Grenoble, Cedex 9, France), *www.esrf.eu/UsersAndScience/Experiments/StructMaterials/ID15/.*
12. M. Di Michiel et al., *Rev. Sci. Instrum.,* 76 (2005), p. 43702.
13. K. Dzieciol, "Four Dimensional Characterization of Creep Cavity Growth in Copper" (Ph.D. Thesis, Ruhr Universität Bochum, 2010).
14. M.E. Kassner and M.T. Pérez-Prado, *Fundamentals of Creep and Alloys* (San Diego, CA: Elsevier, 2004).
15. M.E. Kassner and M.T. Pérez-Prado, *Prog. Mater. Sci.,* 45 (2000), pp. 1–102.
16. V. Levitin, *High Temperature Strain in Metals and Alloys* (Weinheim, Germany: Wiley-VCH Verlag GmbH & Co. KGaA, 2006).
17. O.D. Sherby, R.J. Klundt, and A.K. Miller, *Metall. Trans. A,* 8 (1977), p. 843.
18. K. Dzieciol et al., *EPD Congress 2009,* ed. S. Howard (Warrendale, PA: TMS, 2009), p.15.
19. F. Sket et al., *Mater. Sci. Engng.,* A527 (2010), pp. 2112–2120.
20. F. Sket et al., *Scripta Mater.*, 59 (2008), pp. 558–561.
21. B.J. Cane and G.W. Greenwood, *Metal Sci.,* 9 (1975), pp. 55–60.
22. B.J. Cane, *Metal Sci.,* 13 (1979), pp. 287–294.
23. N.G. Needham and T. Gladman, *Metal Sci.,* 14 (1980), pp. 64–72.
24. N.G. Needham and T. Gladman, *Creep and Fracture of Engineering Materials and Structures*, ed. D. Wilshire and D.R.J. Owen (Swansea, U.K.: Pineridge Press Ltd., 1984), pp. 1263–1276.
25. H. Riedel, *Fracture at High Temperatures* (Berlin, Heidelberg: Springer-Verlag, 1987).
26. A.C.F. Cocks and M.F. Ashby, *Metal Sci.*, 14 (1980), pp. 395–402.
27. A.C.F. Cocks and M.F. Ashby, *Progr. Mater. Sci.,* 27 (1982), pp. 189–244.
28. K. Dzieciol et al., *Acta Mater.,* 59 (2011), pp. 671–677.
29. B. Budiansky, J.W. Hutchinson, and S. Slutsky,*Mechanics of Solids*, ed. H.G. Hopkins and M.J. Sewell (Oxford, U.K.: Pergamon Press, 1982), pp. 13–45.
30. J. Weertman, *J. Appl. Phys.,* 26 (1955), pp. 1213–1217.
31. A.B. Wahab and M.V. Kral, *Mater. Sci. Engng.,* A 412 (2005), pp. 222–229.
32. A. Isaac, "In-situ Tomographic Investigation of Creep Cavity Evolution in Brass" (Ph.D. Thesis, Ruhr University Bochum, 2009).
33. E. Maire et al., *Acta Mater.*, 56 (2008), pp. 4954–4964.
34. J.R. Rice and D.M. Tracey, *J. Mech. Phys. Sol.,* 17 (1969), pp. 201–217.
35. C.I.A. Thomson et al., *J. Mech. Phys. Sol.,* 51 (2003), pp. 127–146.
36. T.J. Marrow et al., *Int. J. of Fatigue,* 26 (2004), pp. 717–725.
37. A.L. Gurson, *J. Engng. Mater. Technol.,* 99 (1977), pp. 2–15.
38. V. Tvergaard and A. Needleman, *Acta Metall.*, 32 (1984), pp. 157–169.

András Borbély, Professor and researcher, and Krzysztof Dzieciol, postdoctoral scholar, are with École Nationale Supérieure des Mines de Saint-Étienne, France; Federico Sket, research associate, is with IMDEA Materials, Madrid, Spain; Augusta Isaac, researcher, is with Brazilian Synchrotron Light Laboratory, Campinas, Brazil; Marco di Michiel, engineer, and Thomas Buslaps, beamline operation manager, are with the European Synchrotron Radiation Facility, Grenoble, France; and Anke R. Kaysser-Pyzalla, chief executive, is with Helmholtz Centre Berlin for Materials and Energy GmbH, Berlin, Germany. Prof. Borbély can be reached at borbely@emse.fr.